JOURNAL OF VIROLOGY, Jan. 2002, p. 379–391 Vol. 76, No. 1
0022-538X/02/$04.00+0 DOI: 10.1128/JVI.76.1.379–391.2002

Rapid and Irreversible CD4$^+$ T-Cell Depletion Induced by the Highly Pathogenic Simian/Human Immunodeficiency Virus $SHIV_{DH12R}$ Is Systemic and Synchronous

Tatsuhiko Igarashi,[1] Charles R. Brown,[1] Russell A. Byrum,[2] Yoshiaki Nishimura,[1] Yasuyuki Endo,[1] Ronald J. Plishka,[1] Charles Buckler,[1] Alicia Buckler-White,[1] Georgina Miller,[3] Vanessa M. Hirsch,[1] and Malcolm A. Martin[1]*

Laboratory of Molecular Microbiology, National Institute of Allergy and Infectious Diseases,[1] and Veterinary Resources Program, Office of Research Services,[3] National Institutes of Health, Bethesda, Maryland 20892,[1] and Bioqual Inc., Rockville, Maryland 20850-3228[2]

Received 2 August 2001/Accepted 1 October 2001

Highly pathogenic simian/human immunodeficiency virus chimeric viruses are known to induce a rapid, irreversible depletion of CD4$^+$ T lymphocytes in the peripheral blood of acutely infected macaque monkeys. To more fully assess the systemic effects of this primary virus infection, specimens were collected serially between days 3 and 21 postinfection from variety of lymphoid tissues (lymph nodes, thymus, and spleen) and gastrointestinal tract and examined by DNA and RNA PCR, in situ hybridization, and immunohistochemical assays. In addition, the lymphoid tissues were evaluated by fluorescence-activated cell sorting. Virus infection was initially detected by DNA PCR on day 3 postinfection in lymph node samples and peaked on day 10 in the T-lymphocyte-rich areas of this tissue. CD4$^+$ T-cell levels remained stable through day 10 in several lymphoid tissue specimens examined but fell precipitously between days 10 and 21. In situ terminal deoxynucleotidyltransferase-mediated dUTP-biotin nick end labeling (TUNEL) assays revealed the accumulation of apoptotic cells during the second week of infection in both lymph nodes and thymus, which colocalized, to a large extent, to sites of both virus replication and CD4$^+$ T-lymphocyte loss.

The signature property of highly pathogenic simian/human immunodeficiency virus chimeric viruses (SHIVs) is their capacity to induce rapid (within 3 to 4 weeks) and irreversible loss of circulating CD4$^+$ T lymphocytes (20, 21, 33). Following the resolution of the acute infection, peak virus loads in the blood rapidly fall 100- to 1,000-fold only to increase again several weeks later (12). Employing confocal microscopy and riboprobes complementary to SIV and HIV sequences, in conjunction with monoclonal antibodies specific for T-cells or macrophages, we recently reported that by week 12 postinfection, high levels (10^6 to 10^7 RNA copies/ml) of virus production in $SHIV_{DH12R}$-infected monkeys are sustained almost entirely by tissue macrophages (19). This unusually rapid and unremitting clinical course is clearly different from that observed for both SIV-infected macaques and HIV-1-infected humans, who develop disease by 1 to 1.5 (22)and 10 (29, 36) years following exposure to virus, respectively.

Nonetheless, because the chimeric virus contains several HIV-1 genes, the lymphocyte subset targeted for elimination (CD4$^+$ T lymphocytes) is identical to that depleted by HIV-1, and the symptoms of the induced immunodeficiency are very similar to that observed in HIV-1-infected individuals, the SHIV-induced disease in macaques can be viewed as a model of human AIDS with a markedly compressed clinical course. The 12- to 20-week infection consists of an acute T-cell phase and a longer macrophage end-stage, with no intervening asymptomatic period commonly associated with HIV-1 and SIV infections. The irreversible loss of CD4$^+$ T cells induced by pathogenic SHIVs eliminates any possibility for a helper T-cell response and is therefore usually accompanied by no virus-specific antibody production (12). Nonetheless, this unremitting and downhill clinical course can be blocked by immunization with specific prophylactic vaccine formulations prior to virus challenge (3, 5) or by administering a potent reverse transcriptase inhibitor during the first week of infection (19). Both approaches preserve CD4$^+$ T-cell function by preventing the acute loss of CD4$^+$ T lymphocytes, thereby ensuring long-term survival of virus-infected animals.

In this study we have focused on the rapid SHIV-induced depletion of CD4$^+$ T cells by serially sacrificing rhesus monkeys on days 3, 5, 7, 10, 14, and 21 postinfection and conducting virologic, biochemical, and immunohistochemical (IHC) analyses of a variety of tissue specimens. Both fluorescence-activated cell sorting (FACS) and IHC analyses indicated that CD4$^+$ T-cell loss from lymphoid tissues began between days 10 and 14 postinfection and was, for the most part, systemically synchronous. Virus-producing cells peaked on day 10 in the T-cell-rich regions of lymph nodes and on day 14 in the thymic medulla and peripheral blood mononuclear cells (PBMC). An in situ immunohistochemical terminal deoxynucleotidyltransferase-mediated dUTP-biotin nick end labeling (TUNEL) assay revealed increased numbers of apoptotic cells in the paracortical regions of lymph nodes that coincided with the presence of virus-producing cells in the same lymph node compartment. The relationship of these results to the subsequent

* Corresponding author. Mailing address: Laboratory of Molecular Microbiology, National Institute of Allergy and Infectious Diseases, National Institutes of Health, 4 Center Dr., Bethesda, MD 20892. Phone: (301) 496-4012. Fax: (301) 402-0226. E-mail: malm@nih.gov.

transition to the late macrophage phase of the SHIV infection are discussed.

MATERIALS AND METHODS

Animal experiments. Rhesus macaques (*Macaca mulatta*), maintained in accordance with the *Guide for the Care and Use of Laboratory Animals* (10), were housed in a biosafety level 2 facility; biosafety level 3 practices were followed. Animals were anesthetized with intramuscular injections of ketamine hydrochloride (Ketaject; Phoenix Pharmaceutical, Inc., St. Joseph, Mo.) and acepromazine maleate (Fermenta Animal Health Co., Kansas City, Mo.) during phlebotomies or SHIV inoculations.

Blood samples were collected in tubes containing EDTA as the anticoagulant. PBMC and plasma samples were prepared and stored at −70°C until use. Lymphocyte immunophenotyping and complete blood counts were also performed from the blood samples. Prior to euthanasia, 150 to 200 ml of blood was drawn from the femoral vein under ketamine anesthesia. Intravenous pentobarbital (Fatal-Plus; Vortech Pharmaceutical, Dearborn, Mich.) (40 mg/kg) was administered for deeper anesthesia. After thoracotomy, the right atrium was incised, and 1,000 ml of sterile heparinized saline (5 U/ml) was infused dropwise into the left ventricle, using a 16-gauge needle attached to infusion tubing. During the perfusion of heparinized saline, fresh tissues were collected for immunophenotyping of lymphocyte subsets by FACS and proviral DNA PCR analysis. Animals were then perfused with 1,000 ml of Carson's modified Millonig's buffered formalin (EMScience, Gibbstown, N.J.), and tissues were collected for histochemical analyses.

Virus. The isolation and characterization of the highly pathogenic $SHIV_{DH12R}$ have been described previously (12, 20). In these experiments, 1×10^5 to 4×10^5 50% tissue culture-infective doses of $SHIV_{DH12R}$ were inoculated intravenously into animals via the saphenous vein. The actual inoculum size administered to each animal is indicated in Table 2.

Virus load measurements. Plasma viral RNA levels were determined by real-time PCR (ABI Prism 7700 Sequence Detection System; Perkin Elmer, Foster City, Calif.) with reverse-transcribed viral RNA from macaque plasma samples as the template (12). Plasma viral RNA was extracted using QIAamp viral RNA kit (Qiagen Inc., Valencia, Calif.) and reverse transcribed with MultiScribe reverse transcriptase (TaqMan reverse transcription reagents kit; Perkin Elmer/Roche, Foster City, Calif.). The cDNA was amplified (45 cycles/default settings) with Ampli*Taq* Gold DNA polymerase (PCR core reagents kit; Perkin Elmer/Roche, Foster City, Calif.) using primer pairs derived from the *gag* gene (forward, nucleotides [nt] 1181 to 1208, and reverse, nt 1338 to 1317) of $SHIV_{DH12}$. $SHIV_{DH12R}$-infected rhesus plasma and $SHIV_{DH12}$-infected rhesus PBMC culture supernatants, previously quantified by the branched-DNA method (11), served as standards for the assay. Proviral DNA was amplified by nested PCR using serially diluted total DNA from 10^6 cells as described previously (40).

Lymphocyte immunophenotyping. EDTA-treated blood samples were stained with fluorochrome-conjugated monoclonal antibodies (CD3-fluorescein isothiocyanate [Serotec Ltd, Oxford, England], CD4-allophycocyanin, CD8-peridinin chlorophyll protein, and CD20-phycoerythrin [Becton Dickinson Immunocytometry Systems, San Jose, Calif.]) and analyzed by FACS (FACSort; Becton Dickinson) as described previously (20).

In situ hybridization. Formalin-fixed, paraffin-embedded tissues were stained for SHIV viral RNA as previously described (18, 19). Briefly, the sections were deparaffinized in water, pretreated with 0.2 N hydrochloric acid–proteinase K, prehybridized, and then hybridized overnight at 51°C with either sense or antisense riboprobe mixture encompassing 90% of the SIV_{mac239} genome plus the *env* gene fragment from $HIV\text{-}1_{IIIB}$ (pBH10, *Eco*RI-*Bam*HI fragment), both conjugated with digoxigenin-UTP (Lofstrand Labs, Ltd., Gaithersburg, Md.) at a final concentration of 1.75 ng/μl. The hybridized sections were then washed in standard posthybridization buffers and RNase solutions (RNase A [R6513; Sigma, St. Louis, Mo.] and RNase T_1 [109 to 193; Roche Molecular Biochemicals, Indianapolis, Ind.]).

The sections were subsequently blocked with 3% normal serum (sheep and horse) in 0.1 M Tris (pH 7.4) and then incubated with sheep antidigoxigenin-alkaline phosphatase (1:500) (Roche Molecular Biochemicals) in serum blocking buffer for 1 h. The sections were rinsed with Tris buffer and reacted with ntiroblue tetrazolium–5-bromo-4-chloro-3-indolylphosphate (NBT/BCIP) (Vector Laboratories, Ltd., Burlingame, Calif.) for 10 h. The samples were rinsed a final time with distilled water, counterstained with 0.1% nuclear fast red (Sigma), washed, dehydrated, and mounted for microscopy. Stained sections were viewed and photographed with a Zeiss Axiophot microscope (Carl Zeiss Inc., Thornwood, N.Y.). Controls for in situ hybridization (ISH) included hybridizing SHIV-infected macaque lymph node with the digoxigenin-UTP sense riboprobe, hybridizing uninfected lymph node with the antisense riboprobe, and substituting phosphate-buffered saline (PBS) (sheep antidigoxigenin-alkaline phosphatase) for the primary antibody.

IHC. Sections from Formalin-fixed paraffin-embedded tissues were stained with an anti-human CD4 mouse monoclonal antibody (NCL-CD4; Novacastra Laboratories, Ltd., London, United Kingdom). Sections were rehydrated and processed for 6 to 8 min in a Presto pressure cooker (National Presto Industries, Inc. Eau Claire, Wis.) in 1 mM EDTA (pH 8.0) to unmask CD4 antigen. The samples were sequentially treated with PBS, aqueous hydrogen peroxide, serum block (3% normal goat serum, 1% nonfat milk, and 0.5% bovine serum albumin), and the anti-CD4 monoclonal antibody (1:40) for 1 h. The reaction was visualized using the Vectastain Mouse-IgG Peroxidase ABC kit (Vector Laboratories) and diaminobenzidine (DAB) followed by 10 s of treatment in DAB enhancing solution (Vector Laboratories, Ltd.). Samples were then rinsed in distilled water and counterstained with hematoxylin (Sigma).

Tissue sections were also stained with a monoclonal antibody against macrophages, HAM56 (DAKO Corporation, Carpinteria, Calif.). This antibody was detected with the ABC-alkaline phosphatase method (Vector Laboratories, Ltd.) as outlined above and Vector Red substrate (Vector Laboratories, Ltd.).

Apoptosis assay. A TUNEL assay kit, TACS 2 TdT-DAB (Trevigen, Inc., Gaithersburg, Md.), was used to identify cells undergoing apoptosis in Formalin-fixed, paraffin-embedded tissue sections. Deparaffinized tissue sections were digested for 15 min. with 25 μg/ml of proteinase K at 37°C, rinsed in distilled water, and quenched in a methanol-hydrogen peroxide solution for 6 min. The sections were reacted with a biotinylated TdT deoxynucleoside triphosphate (dNTP) solution containing a manganese cation for 60 min at 37°C. The incorporated TdT dNTP was detected using a streptavidin-horseradish peroxidase (HRP) reagent (Trevigen, Inc.) at a 1:50 dilution for approximately 10 min. Stained sections were rinsed in water, counterstained with hematoxylin, mounted, and photographed. Controls included omission of the TdT enzyme and/or streptavidin-HRP conjugate, TACS-Nuclease (Trevigen, Inc.)-treated tissues, and staining of uninfected tissue sections.

RESULTS

$SHIV_{DH12R}$ induces extremely rapid and irreversible depletion of $CD4^+$ T lymphocytes within weeks of inoculation of rhesus monkeys and death due to complications related to immunodeficiency within 3 to 6 months (12). To more fully evaluate this unusual pattern of $CD4^+$ T-cell loss systemically, animals inoculated with 1×10^5 to 4×10^5 $TCID_{50}$ of virus, were serially sacrificed during the first 21 days of infection. As indicated in Materials and Methods, the infected monkeys were initially perfused with heparinized saline to obtain specimens for FACS and proviral DNA PCR analyses, and following Formalin perfusion, tissues were collected for IHC studies and ISH.

Viral RNA levels were measured in plasma samples collected from each animal prior to the time of euthanasia. As shown in Fig. 1a, approximately 10^5 copies of viral RNA/ml were detected in the blood within 3 days of $SHIV_{DH12R}$ inoculation. The kinetics of virus infection in the inoculated macaques was very similar for the six animals under study, with peak viral RNA levels occurring between days 10 and 15 (only measured in monkeys AE56 and BD35, sacrificed on days 14 and 21, respectively). These kinetics are in good agreement with that previously reported for long-term $SHIV_{DH12R}$ infections of rhesus monkeys (12).

Levels of proviral DNA and $CD4^+$ T lymphocytes in lymphoid tissues. Viral replication in lymphoid tissues was initially evaluated by performing quantitative proviral DNA PCR on lysates prepared from cell suspensions. Contamination of these samples by circulating infiltrating lymphocytes was minimized by whole-animal heparin/saline perfusion prior to tissue collection. Low levels of viral DNA was detected in inguinal, mesenteric, and colonic lymph nodes (0.6, 1.5, and 1.8 DNA

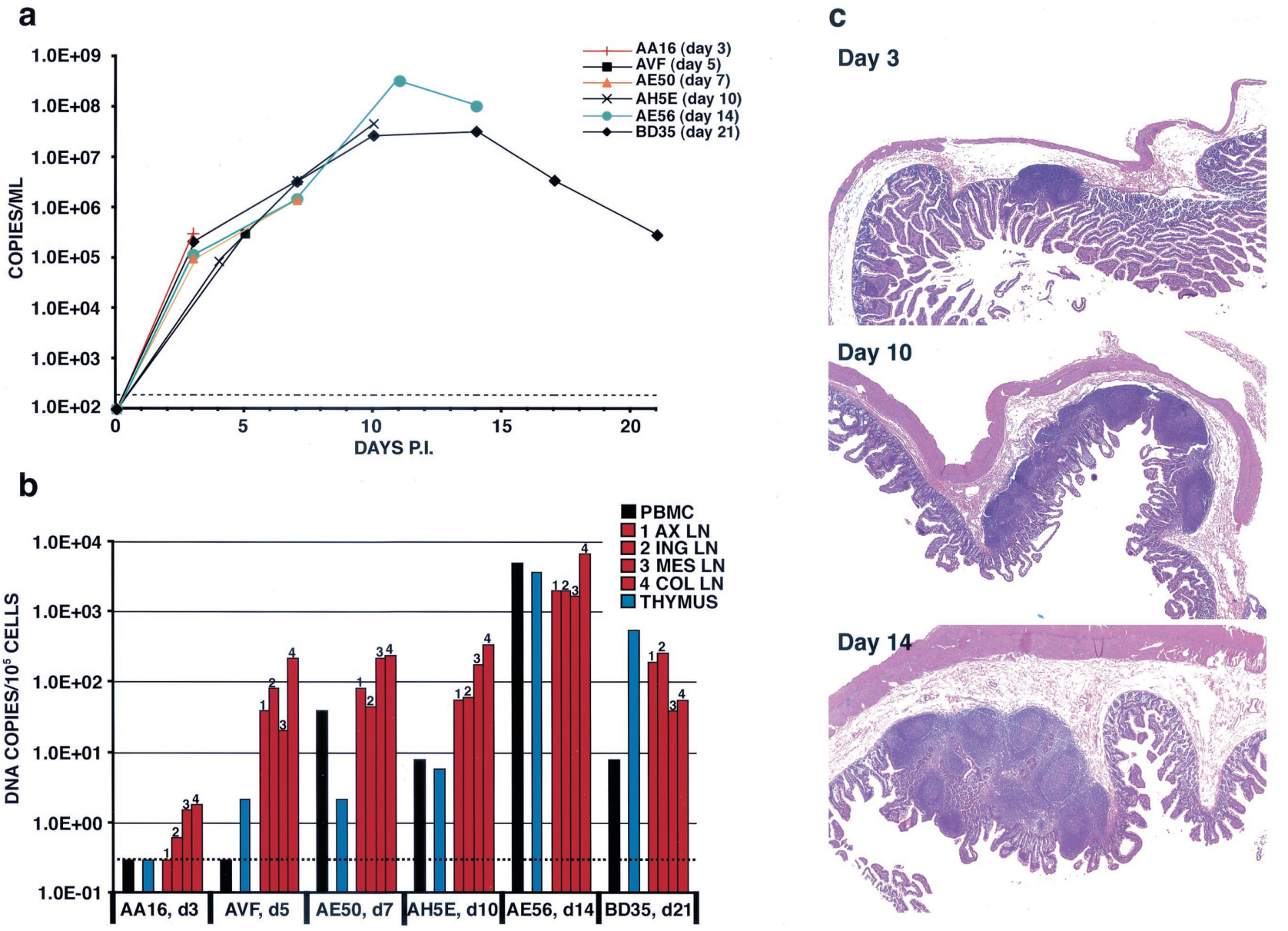

FIG. 1. Viral loads and general histopathological changes associated with acute SHIV$_{DH12R}$ infection. (a) Plasma viral RNA levels were determined by real-time RT-PCR up to the day of sacrifice using primer pairs mapping to the SIV *gag* sequences. (b) Cell-associated viral DNA present in PBMC, lymph nodes (LN), and thymus samples was determined by nested DNA PCR using *gag* primers to amplify serially diluted total DNA samples prepared from PBMC and the indicated lymphoid tissues. AX LN, axillary lymph node; ING LN, inguinal lymph node; MES LN, mesenteric lymph node; COL LN, colonic lymph node. (c) Hematoxylin- and eosin-stained sections of ileum collected on days 3, 10, and 14 postinfection (P.I.). Original magnification, ×6.4.

copies/10^5 cells, respectively) on day 3 postinfection (Fig. 1b), a time at which approximately 10^5 viral RNA copies/ml were measured in the blood of four of the infected rhesus monkeys (Fig. 1a). The cell-associated viral DNA loads increased 100-fold in lymph nodes between days 3 and 5 and stabilized at that level (approximately 100 DNA copies/10^5 cells) through day 10. Peak proviral DNA levels were reached on day 14 in all of the lymphoid tissues examined (1,680 to 6,880 DNA copies/10^5 cells) as well as in PBMC (4,900 DNA copies/10^5cells). Compared to lymph nodes, virus replication in the thymus was delayed but, by day 14, was similar (3,610 DNA copies/10^5 cells) to that measured in lymph node samples.

Changes in lymphocyte subsets in blood and lymphoid tissue as a consequence of the $SHIV_{DH12R}$ infection were monitored by FACS on specimens collected immediately following the saline/heparin perfusion. For each animal, the lymphocyte subset profiles obtained were compared to the preinfection FACS analysis of PBMC and inguinal lymph node samples. As shown in Table 1, no appreciable changes in T- or B-cell subsets occurred during the first 10 days of infection. By day 14, however, significant $CD4^+$ T-cell depletion was observed in the peripheral blood and lymph nodes. The $CD4^+$ T-cell loss became even more marked by day 21, reduced by nearly 90% in both the blood and multiple lymph nodes.

Pathologic changes accompanying acute $SHIV_{DH12R}$ infection. The significant histopathological findings in the hematoxylin- and eosin-stained tissue sections from the six animals sacrificed between days 3 and 21 of infection are summarized in Table 2. During this period, the changes observed affected lymphoid tissues (lymph nodes, thymus, gut-associated lymphoid tissue [GALT], and spleen) primarily and became apparent on day 5 postinfection. The early changes observed included lymphoid hyperplasia and expansion of germinal centers in lymph nodes and GALT, progressing to increased numbers and distortion of the germinal centers by days 10 to 14 (this is shown for the GALT in Fig. 1c).

Between days 14 and 21, disorganized and involuted germinal centers accompanied by infiltrating neutrophils and expansion of paracortical regions was observed. Histopathological changes in the thymus, affecting primarily the cortex, were not evident until day 14 and progressed to marked depletion of cortical lymphocytes by day 21. It is worth noting that all $SHIV_{DH12R}$-infected animals, sacrificed at later times (between weeks 12 and 26) because of severe diarrhea or marked weight loss had no discernible thymus or only thymic remnants embedded in mediastinal fatty tissue at the time of autopsy.

IHC/ISH studies of sequential lymph node and GI tract samples. PCR analyses of viral RNA loads in the blood and DNA levels in lymphoid tissues indicated that $SHIV_{DH12R}$ replication was rapid and synchronous. Furthermore, FACS analyses of blood and tissue suspensions revealed that the virus-induced $CD4^+$ T-lymphocyte depletion was systemic, affecting multiple lymphoid compartments, with the major loss of cells occurring between days 10 and 21 postinfection. To further characterize the cytopathic effects and viral replication events occurring within lymphoid tissues, IHC and ISH evaluations of lymph node specimens were carried out. In these analyses, inguinal, axillary, mesenteric, and colonic lymph nodes were examined in animals sacrificed at various times postinfection. Since all lymph node specimens exhibited tem-

TABLE 1. T-cell subset changes in $SHIV_{DH12R}$-infected animals[a]

Animal ID (day of sacrifice)	Tissue	% of cells			
		$CD3^+$	$CD3^+CD4^+$	$CD3^+CD8^+$	$CD20^+$
AA16	PBMC (pre)	73	41	44	16
(3)	PBMC	81	47	37	13
	Inguinal LN (pre)	66	44	28	35
	Inguinal LN	73	47	28	30
	Mesenteric LN	59	41	22	41
	Colonic LN	78	50	29	25
	Pancreatic LN	77	43	36	18
	Spleen	56	26	33	41
AVF	PBMC (pre)	71	48	40	24
(5)	PBMC	74	50	38	19
	Inguinal LN (pre)	64	46	23	37
	Inguinal LN	67	47	35	36
	Axillary LN	66	45	38	36
	Colonic LN	86	65	25	17
	Spleen	49	23	48	51
AE50	PBMC (pre)	58	34	30	35
(7)	PBMC	60	37	25	36
	Inguinal LN (pre)	71	45	26	32
	Inguinal LN	51	34	23	50
	Axillary LN	56	41	20	44
	Mesenteric LN	65	40	27	35
	Colonic LN	69	49	21	33
	Spleen	33	15	21	63
AH5E	PBMC (pre)	55	31	35	36
(10)	PBMC	60	30	34	33
	Inguinal LN (pre)	59	45	22	45
	Inguinal LN	53	41	17	49
	Axillary LN	63	47	22	40
	Mesenteric LN	49	38	18	52
	Colonic LN	47	38	16	55
	Spleen	35	17	23	65
AE56	PBMC (pre)	56	37	33	30
(14)	PBMC	52	**14**	54	28
	Inguinal LN (pre)	67	51	21	34
	Inguinal LN	36	**26**	26	63
	Axillary LN	33	**11**	25	66
	Mesenteric LN	54	**15**	42	45
	Colonic LN	58	**13**	43	41
	Spleen	36	**21**	38	53
BD35	PBMC (pre)	73	46	34	21
(21)	PBMC	55	**5**	67	22
	Inguinal LN (pre)	67	62	19	35
	Inguinal LN	66	**8**	58	35
	Axillary LN	66	**7**	57	34
	Submandibular LN	57	**7**	48	42
	Mesenteric LN	60	**7**	52	41
	Colonic LN	65	**7**	55	35
	Pancreatic LN	59	**7**	51	42
	Spleen	58	**3**	54	32

[a] LN, lymph node. Values in bold represent significant reduction compared to preinfection value.

TABLE 2. Data for individual animals

Animal ID	Sex	Age (yr)	Inoculum size (10^5 $TCID_{50}$)	Day p.i.	Histopathological findings
AA16	F	3	1.0	3	Indistinguishable from uninfected animals
AVF	M	4	4.1	5	Axillary LN: focal expansion and distortion of germinal centers Thymus: within normal limits Duodenum: prominent germinal centers in the GALT
AE50	F	3	1.0	7	Mesenteric LN: lymphoid hyperplasia with focal expansion of paracortex Cecum: diffuse and moderate hyperplasia of the GALT Thymus: within normal limits
AH5E	F	3	1.0	10	Mesenteric, colonic LN: lymphoid hyperplasia with numerous large active germinal centers Duodenum, jejunum, ileum: hyperplasia of the GALT Thymus: within normal limits
AE56	F	3	1.0	14	Mesenteric LN: lymphoid hyperplasia with numerous cortical and paracortical follicles, many with depleted germinal centers Ileum: hyperplasia of the GALT with prominent active germinal centers Thymus: mild cortical depletion
BD35	M	2	3.0	21	Multiple LN: lymphadenopathy with follicular hyperplasia, paracortical expansion, and multifocal neutrophilic infiltrates and erythrophagocytosis Thymus: mild and diffuse cortical lymphoid depletion

porally similar cytological changes and levels of virus replication, we elected to show only the results from mesenteric lymph nodes, both for consistency and because of their central location anatomically.

The staining properties and location of CD4$^+$ T cells in a mesenteric lymph node of an uninfected animal are shown in Fig. 2a. As expected, the CD4$^+$ T lymphocytes were homogeneously distributed in the paracortical and cortical regions and were only rarely seen in B-cell-rich germinal centers. By day 7 postinfection, the lymph node germinal centers became more prominent and were surrounded by increased numbers of CD4$^+$ T cells (Fig. 2b). The marked expansion of lymph node germinal centers on day 10 was associated with further clustering of the CD4$^+$ T lymphocytes (Fig. 2c). By day 14, the numbers of CD4$^+$ T cells in the paracortex was noticeably reduced (Fig. 2d), consistent with the results of FACS analyses performed on the same clinical specimen. Similar IHC staining of CD8$^+$ and CD20$^+$ lymphocytes in serially collected lymph node specimens revealed that the numbers of neither subset changed significantly during the first 3 weeks of the SHIV$_{DH12R}$ infection (data not shown). Taken together, the IHC and FACS analyses of lymph node samples were in good agreement and indicated that CD4$^+$ T cells were specifically depleted in lymph nodes between days 10 and 14 postinfection.

Viral RNA synthesis in mesenteric lymph nodes was examined by ISH using riboprobes encoding both SIV and HIV-1

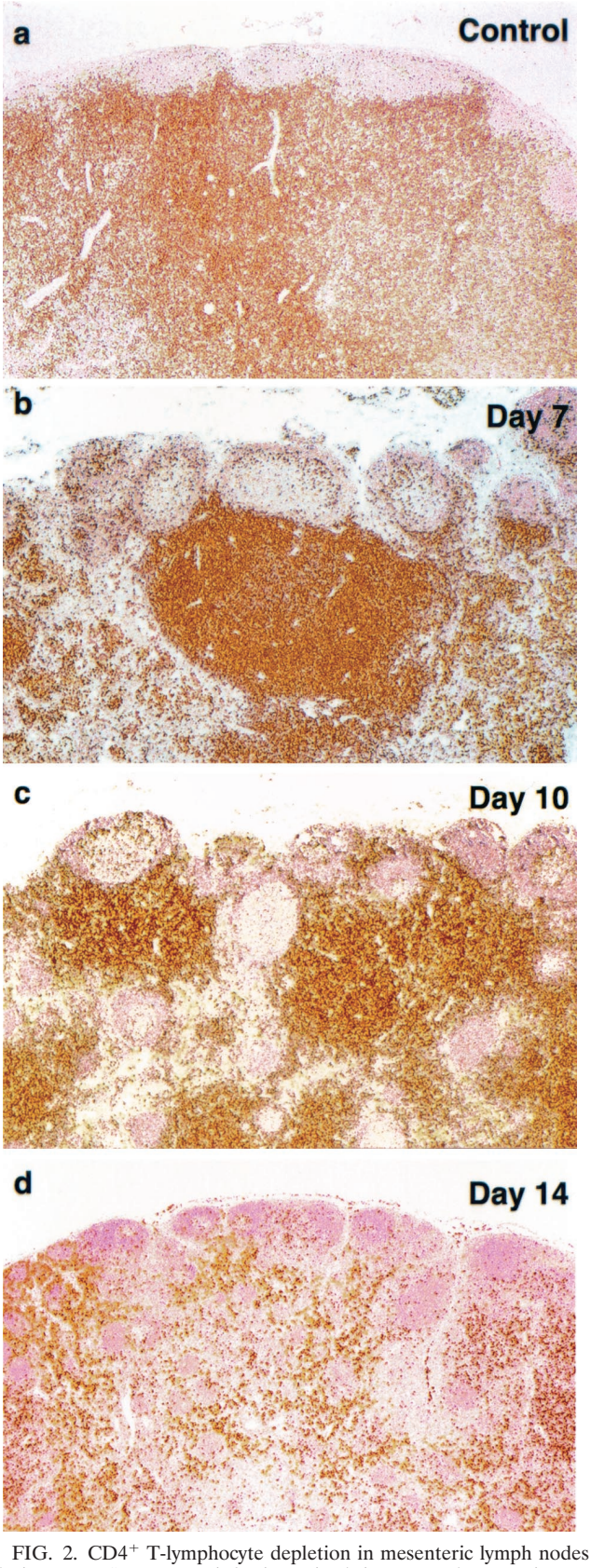

FIG. 2. CD4$^+$ T-lymphocyte depletion in mesenteric lymph nodes during acute SHIV$_{DH12R}$ infection. Fixed tissue samples were immunostained with an anti-human CD4 mouse monoclonal antibody at the indicated times. Original magnifications: a, ×5; b, ×5; c, ×5; d, ×4.

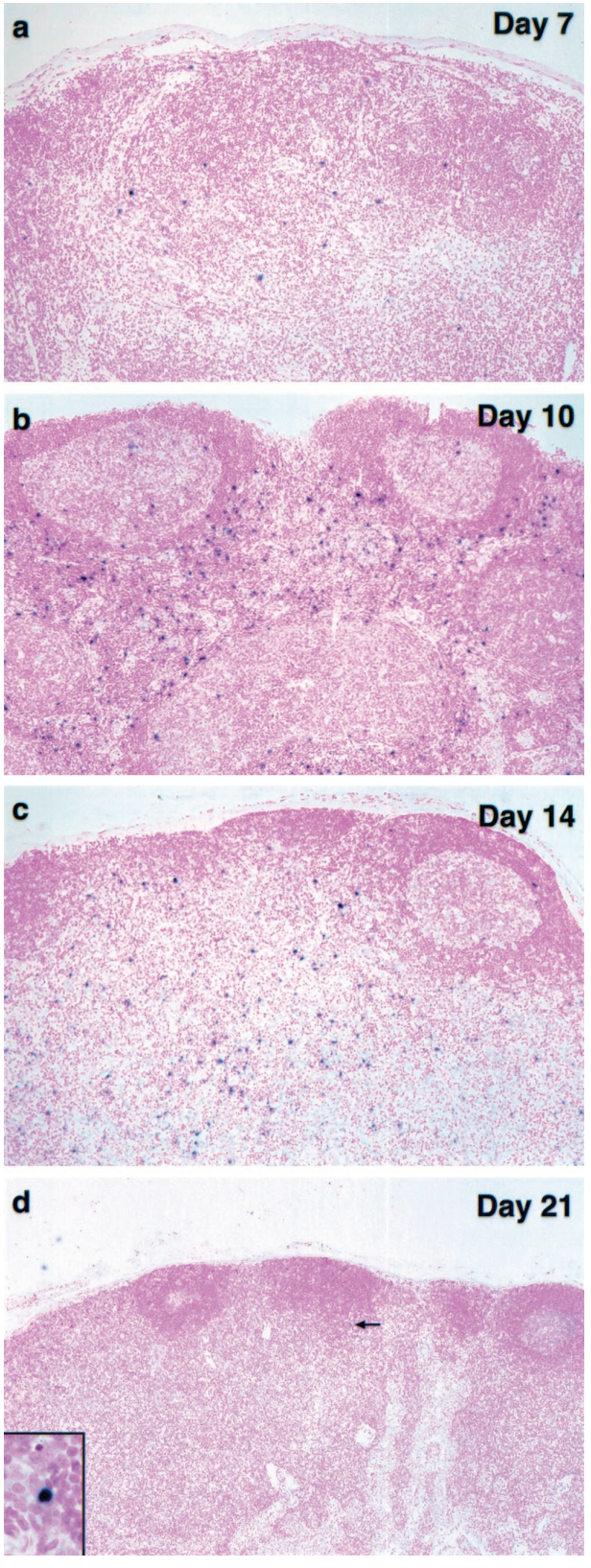

FIG. 3. Viral replication in mesenteric lymph nodes during acute $SHIV_{DH12R}$ infection. Mesenteric lymph node samples were analyzed by ISH at the indicated times using antisense riboprobes specific for both HIV and SIV sequences. Original magnifications: a, ×10; b, ×10; c, ×10; d, ×10; inset, ×40.

env sequences. $SHIV_{DH12R}$ RNA was initially detected in the cortical and paracortical regions on day 7 and peaked on day 10 postinfection (Fig. 3a and b). Reduced levels of viral RNA production were measured on day 14 and were associated with marked lymphocyte depletion in the paracortex, as revealed by counterstaining (Fig. 3c). The latter was temporally consistent with the reduced numbers of $CD4^+$ T cells detected by IHC (Fig. 2). In all cases, the small round ISH-positive cells resembled lymphocytes morphologically and were localized to the T-cell-rich areas of the lymph node. By day 21, levels of viral RNA synthesis, as measured by ISH, became minimally detectable (Fig. 3d).

$SHIV_{DH12R}$ RNA was also detected in the lamina propria and GALT from a sample of ileum as early as day 7 postinfection (Fig. 4a). ISH-positive cells were also present in a section of the cecum collected on day 14 (Fig. 4b). Vigorous viral RNA synthesis was also observed on day 10 in the periarteriolar lymphoid sheath region of the spleen (Fig. 4c). On day 14, the level of viral RNA production decreased (Fig. 4d), a result similar to that observed in mesenteric lymph nodes (Fig. 3)

The rapid and synchronous nature of the $CD4^+$ T-lymphocyte loss in the $SHIV_{DH12R}$-infected animals provided a unique opportunity to monitor the process of virus-induced cell killing in vivo. For HIV-1, the voluminous literature on this subject includes direct cell lysis by virus (6, 14), syncytium formation (27, 48), and a variety of apoptotic mechanisms (2, 4, 16, 28, 30, 46). Apoptosis has been proposed to be responsible for the death of both virus-infected and uninfected cells (13, 15), the latter reflecting the so-called "bystander effect."

An in situ TUNEL assay was used to visualize apoptotic cells in fixed lymph node specimens collected from the infected macaques (Fig. 5). The day 3 sample contained very few TUNEL-positive cells, which were primarily located in germinal centers. A similar pattern was seen in a lymph node section from an uninfected control monkey (not shown). By day 10, the number of apoptotic cells had increased significantly, and they were located in both germinal centers and paracortical regions. In general, the TUNEL-positive cells on day 10 were small, with morphological features typical of lymphocytes. On day 14, fewer apoptotic cells were present but they were significantly larger than those seen earlier; the latter were particularly prominent in germinal centers. Interestingly, these large cells contained multiple TUNEL-positive pyknotic nuclei in their cytoplasm, whereas their own nucleus was TUNEL negative (Fig. 5c, inset). These cells resembled macrophages in the process of phagocytosing apoptotic lymphocytes.

Apoptosis in $CD3^+/CD4^+$ cells in the blood and lymph nodes was also evaluated by FACS using cell suspensions of axillary and inguinal lymph node specimens collected serially from a single rhesus macaque (AN83) on days 9, 12, 13, and 14 postinfection. The levels of annexin V-positive $CD4^+$ T cells from five uninfected animals averaged 2.9% from both sources. A modest two- to threefold increase in apoptotic $CD4^+$ T lymphocytes was measured in blood and lymph node samples beginning on day 12 postinfection (data not shown).

Collectively, these results are most consistent with the replication of $SHIV_{DH12R}$ in the T-cell zone and inducing apoptosis of $CD4^+$ T lymphocytes located in this lymph node

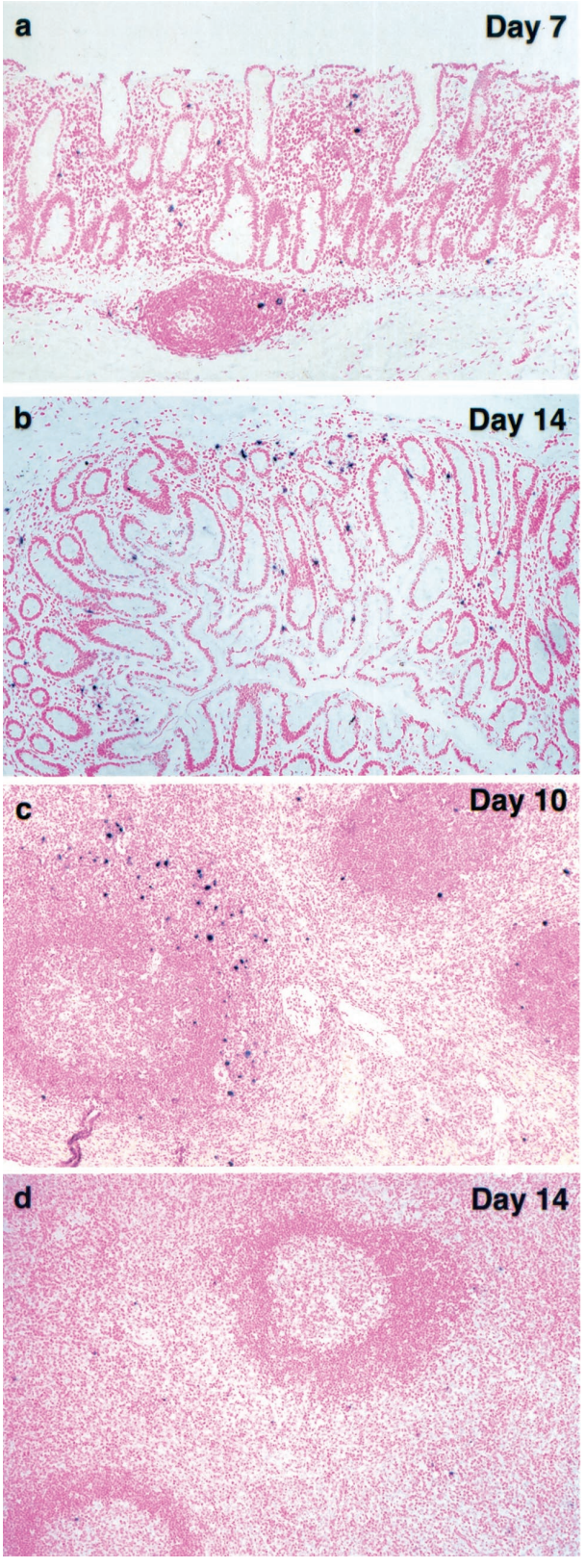

FIG. 4. Viral replication in spleen and gastrointestinal tract during acute SHIV$_{DH12R}$ infection. Ileum (a), cecum (b), and spleen (c and d) samples were analyzed by ISH at the indicated times using antisense riboprobes specific for both HIV and SIV sequences. Original magnifications: a, ×12; b, ×12.5; c, ×10; d, ×10.

compartment. To better understand the nature of the apoptotic cells present in the germinal centers and the population dynamics of other cell types within lymph nodes during the acute viral infection, serial specimens were stained with the macrophage-specific monoclonal antibody HAM56. Both bright-field and UV-enhanced images were obtained from the stained tissues (Fig. 6).

Compared to the low basal level of HAM56-positive cells present on day 3, the numbers of macrophages found in lymph node germinal centers increased enormously by day 7 (Fig. 6a and b). In the context of the acute SHIV$_{DH12R}$ infection, this profound increase in macrophages was unexpected because it was observed within a lymph node compartment rich in B cells in which little if any viral replication occurred (see Fig. 3). By day 14, however, the distribution of HAM56-positive cells shifted away from the germinal centers (Fig. 6c). Over the next week, the latter pattern became even more pronounced, so that on day 21 postinfection, large numbers of macrophages were present in all lymph node regions. These results indicate that prior to peak virus replication, macrophages initially accumulate in germinal centers and are subsequently found in the paracortical regions coincident with the marked depletion of the CD4$^+$ T-cell population.

Effect of acute SHIV$_{DH12R}$ infection on the thymus. Infection of the thymus by both HIV-1 and SIV contributes to the loss of CD4$^+$ T lymphocytes and the development of disease. Although studies of HIV-1 have focused primarily on thymocytes in the SCID-hu mouse (25, 39, 41, 42), infections of infants have been reported to induce marked thymic involution, depletion of mature and immature thymocytes, and rapid progression to AIDS (31, 32, 34). The thymus is also a primary target during SIV infections of juvenile rhesus monkeys, when it undergoes increased thymocyte apoptosis and depletion of progenitor cell types (26, 35, 47).

Although the proviral DNA load eventually reached levels comparable to those seen in other lymphoid tissues, SHIV$_{DH12R}$ replication in the thymus was delayed (see Fig. 1b). This slower pace of thymus infection was also reflected in ISH studies measuring viral RNA synthesis (Fig. 7). The extremely low numbers of virus-positive cells in the thymic medulla on day 10 (compare to the day 10 mesenteric lymph node from the same animal in Fig. 3b) increased greatly by day 14 postinfection (Fig. 7c). Although the majority of viral RNA-producing cells were located in the medulla, some ISH-positive cells were also present in the cortex.

IHC analysis of CD4$^+$ T lymphocytes revealed profound depletion of these cells from the thymic medulla between days 10 and 14 and further loss by day 21 (Fig. 7). Not unexpectedly, TUNEL assay of infected thymus tissue revealed significant numbers of apoptotic cells in the cortex on day 3 postinfection, the site of maturing T lymphocytes. This pattern is similar to that observed in the cortex of uninfected monkeys (not shown). On day 10, the frequency of apoptotic cells increased modestly and remained confined primarily to the cortex. However, by day 14, the number of TUNEL-positive cells increased significantly (Fig. 7). These apoptotic cells were found not only in the cortex, but for the first time were also present in the medulla, the site of robust virus replication in the thymus (Fig. 7c).

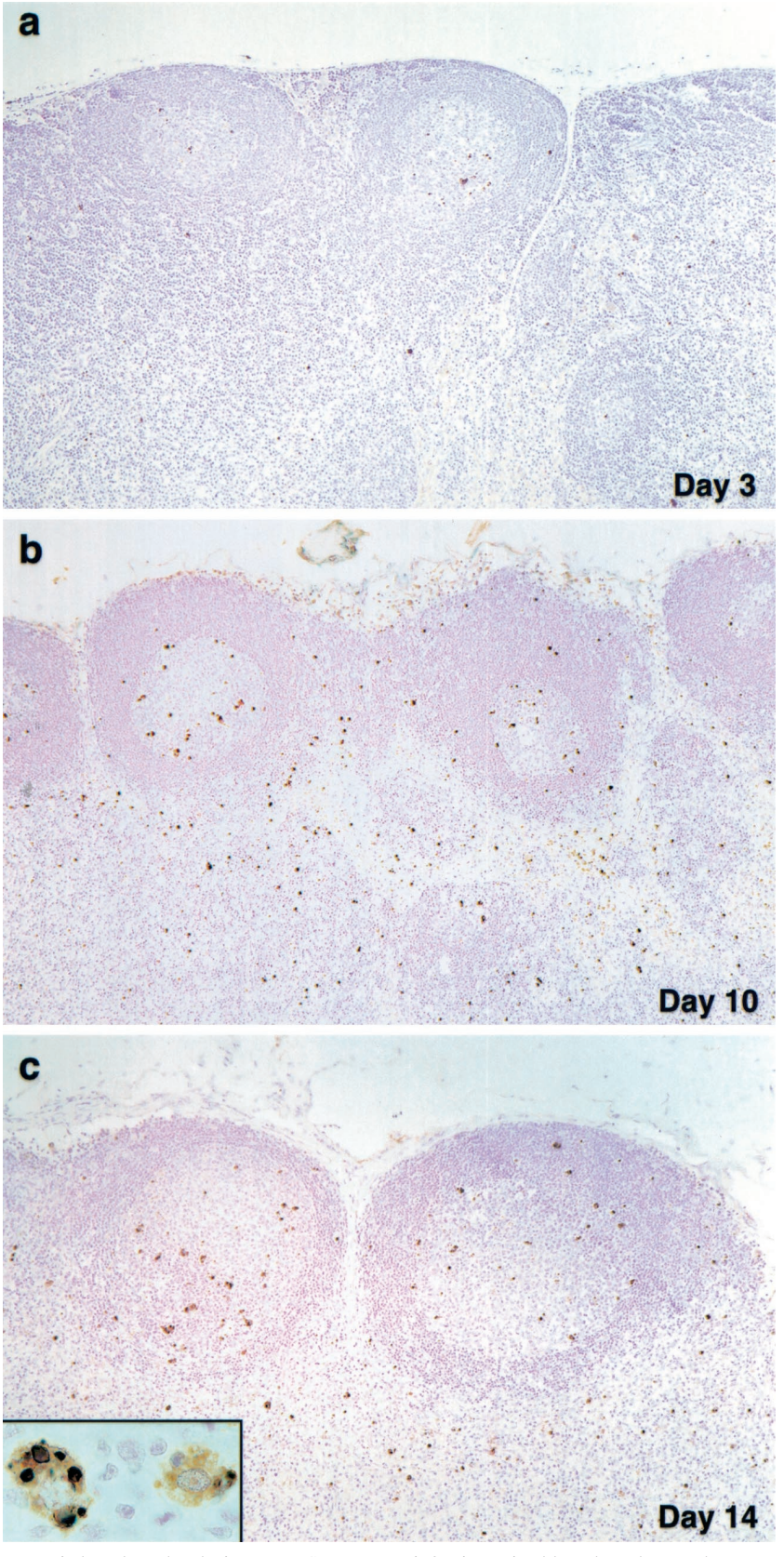

FIG. 5. Apoptosis in mesenteric lymph nodes during acute $SHIV_{DH12R}$ infection. Fixed lymph node samples were subjected to TUNEL assay at the indicated times postinfection. In the absence of TdT/dNTP or the streptavidin-HRP conjugate, no staining was observed. The reactivity of uninfected lymph node samples was similar to the day 3 specimen (not shown). Original magnifications: ×10 (inset, ×63).

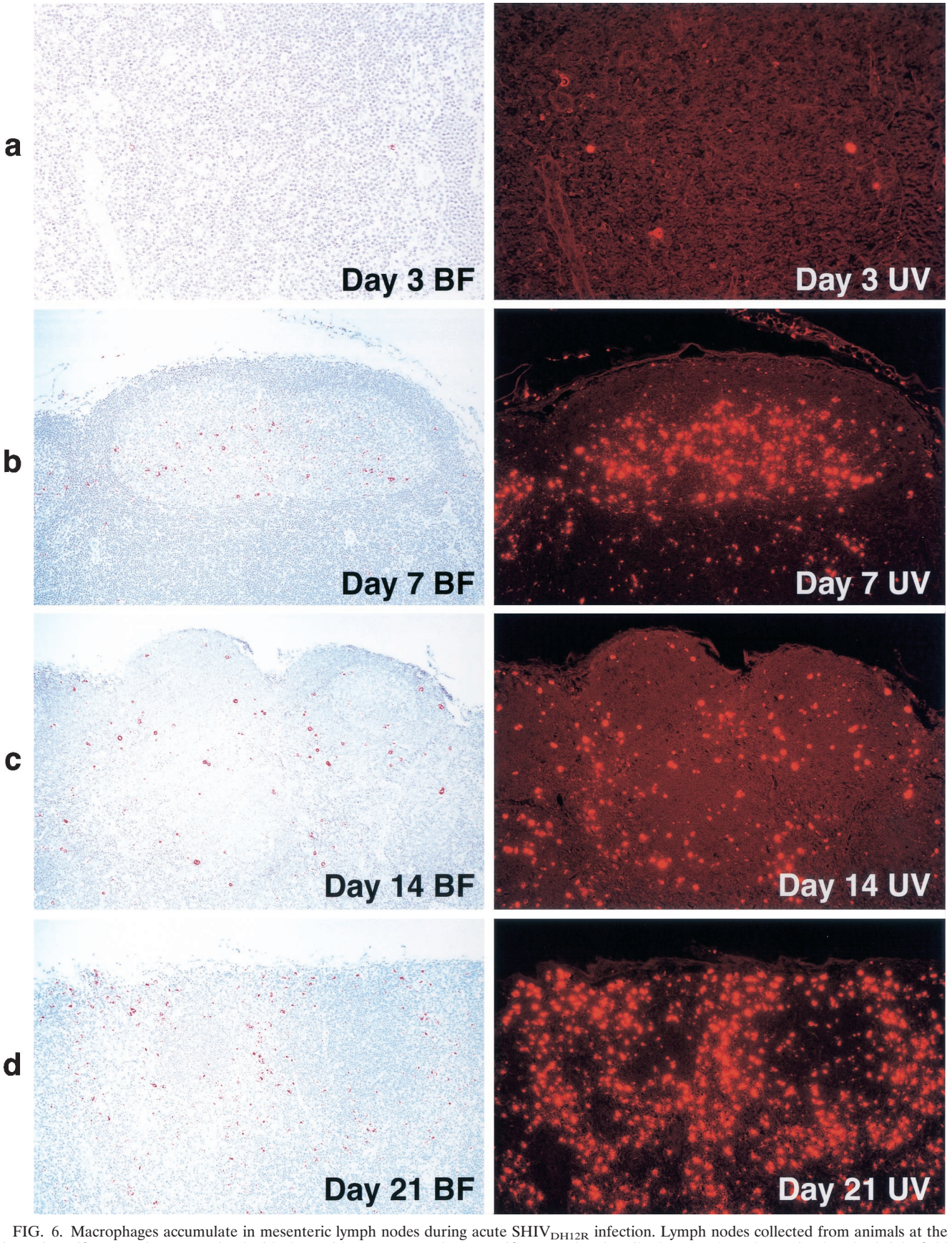

FIG. 6. Macrophages accumulate in mesenteric lymph nodes during acute $SHIV_{DH12R}$ infection. Lymph nodes collected from animals at the time of sacrifice were immunostained with the anti-human macrophage-specific monoclonal antibody HAM56 and examined under bright-field (BF) conditions (left panels) or following UV enhancement (right panels). Original magnifications: a, ×20; b, c, and d, ×10.

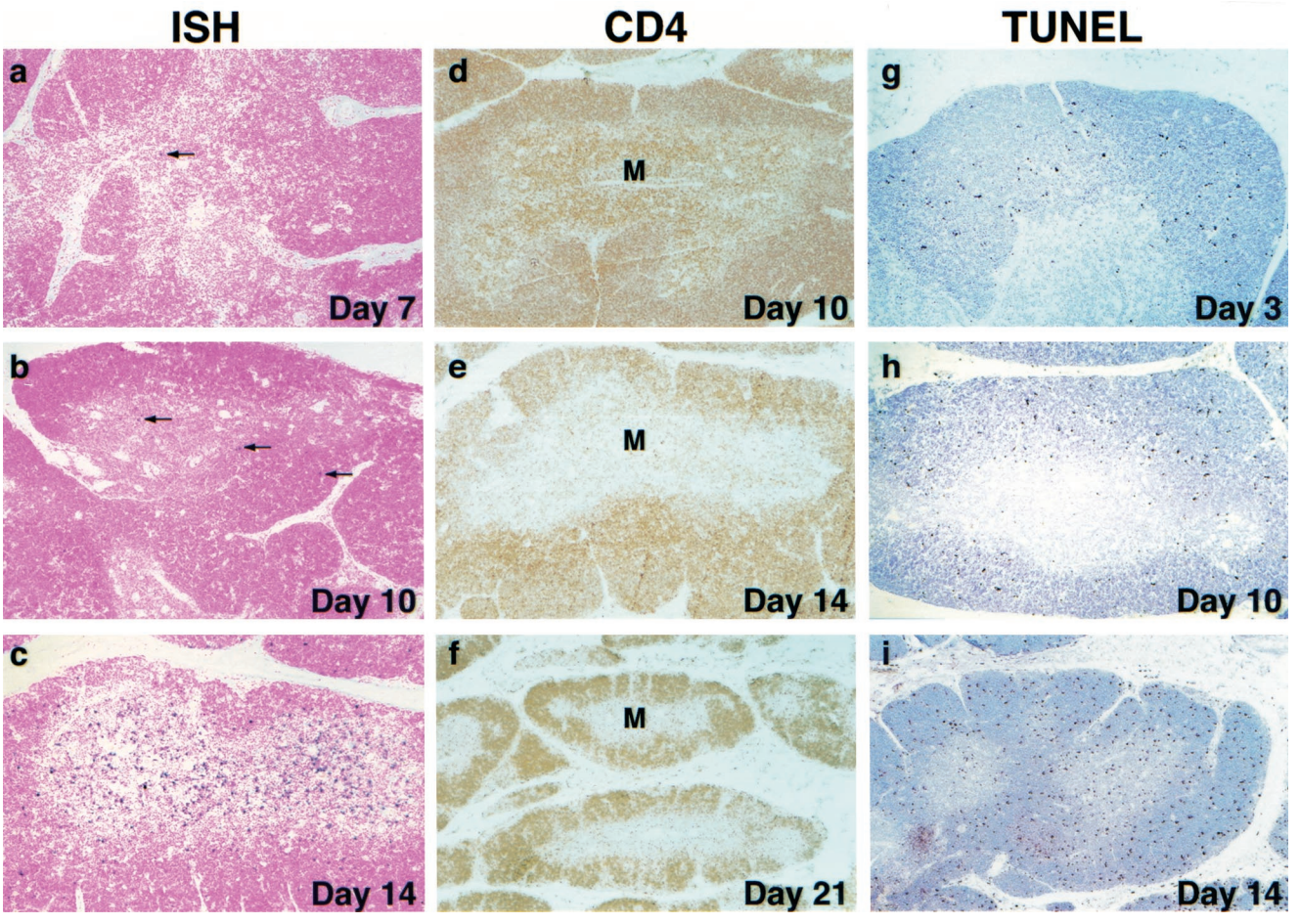

FIG. 7. Virus replication, $CD4^+$ T-cell depletion, and apoptosis in the thymus during acute $SHIV_{DH12R}$ infection. ISH, CD4 T-cell immunohistochemistry, and TUNEL assays were performed on sections of thymus collected at the indicated times. The arrows indicate the few ISH-positive cells on days 7 and 10. Original magnifications: a, b, c, g, and h, ×10; d, e, and i, ×5; f, ×4. M, medulla.

DISCUSSION

The analysis of the acute $SHIV_{DH12R}$ infection described in this report generated both anticipated and unexpected results. The synchronous loss of $CD4^+$ T lymphocytes was indeed systemic, affecting multiple lymphoid compartments (lymph nodes, GI tract, and thymus). Virus replication, for the most part, was also systemically synchronous, although viral RNA synthesis, as measured by ISH, was delayed somewhat in the thymus compared to lymph nodes. The latter finding very likely reflects the limited trafficking of mature T cells through the thymus (1, 43). The few infected circulating lymphocytes which eventually reached the thymus were able to establish a robust infection very rapidly, causing a marked reduction of $CD4^+$ thymocytes cells by day 14. The rise and fall of virus loads in the blood followed on the heels of similar events in lymphoid tissues in a process that seemed to be limited solely by the number of remaining $CD4^+$ lymphocytes.

In contrast, the infected-cell dynamics, as measured by levels of proviral DNA in lymphoid tissues during the acute phase of SHIV infections, was more difficult to interpret, especially when considered together with the amounts of progeny virions released contemporaneously into the circulation (plasma viral RNA loads) and the analyses of lymphocyte subsets in the same tissues. Cell-associated viral DNA determinations are currently viewed with some skepticism primarily because of the presence of defective DNA copies in some long-lived $CD4^+$ T-cell populations. However, the cell-associated viral DNA detected during the initial 2 to 3 weeks of the SHIV infection represents recently synthesized reverse transcripts and is most likely present in cells actively producing virus. Thus, our failure to measure increasing numbers of $SHIV_{DH12R}$-infected cells in lymph node specimens collected between days 5 and 10 (Fig. 1b) seemed somewhat incongruous because it occurred during a period when plasma viral RNA levels were increasing more than 100-fold (Fig. 1a) and the number of $CD4^+$ T cells remained relatively stable (Table 1 and Fig. 2).

One explanation for the seemingly stable levels (0.1% of total lymph node cells) of virus-producing lymphocytes is related to the lymphadenopathy (palpable inguinal and axillary lymph nodes) which appeared in $SHIV_{DH12R}$-infected animals during this period (days 5 to 10 postinfection). This increase in lymph node volume is indicative of a rapid influx and/or proliferation of cells. The source and precise identity of these cells remain to be determined, but since the FACS analyses presented in Table 1 indicated no significant change in lymphocyte subsets during this period, it must be concluded that the num-

bers of both CD4$^+$ and CD8$^+$ T cells and CD20$^+$ B cells had increased substantially. The net effect of this process would "dilute" the number of virus-producing lymph node cells, thereby masking any demonstrable increase in the infected cell population. This phase of the acute SHIV$_{DH12R}$ infection lasted until day 10 to 12 postinfection; by day 14, CD4$^+$ T cells could no longer be replenished systemically, and a 10-fold increase in proviral DNA levels was measured. This was associated with marked losses of CD4$^+$ T cells from lymphoid tissue and blood.

The replicative and cytopathic properties of SHIV$_{DH12R}$ in the thymus were quite similar to those reported previously for a pathogenic SIV strain (SIV$_{mac239}$) during acute infections of juvenile rhesus monkeys (26, 47). The majority of the SIV-producing cells were located in the thymic medulla, the primary site of virus replication. By day 50, the pathogenic SIV$_{mac239}$ had induced a marked decrease of both CD4 and CD8 singly positive T lymphocytes, reflecting, in part, a rebound in the number of CD4$^+$/CD8$^+$ and CD34$^+$ thymocyte precursors in the thymus at 7 weeks postinfection. While SHIV$_{DH12R}$ also primarily targeted thymic medullary cells, its cytopathic effect on single positive CD4$^+$ T cells was both rapid and irreversible; no replenishment of this thymocyte subset was observed. Only thymic remnants were found in SHIV$_{DH12R}$-infected animals at the time of euthanasia, usually 12 to 24 weeks postinfection.

In contrast to the replication pattern and pathogenic effects of SHIV$_{DH12R}$ in the rhesus thymus, studies of HIV-1 infections of human thymocytes have yielded conflicting results. HIV-1 has been reported to infect mature (32) and immature (34) thymocytes in specimens analyzed from seropositive infants. In SCID-hu mice engrafted with human fetal thymus/liver tissue, HIV-1 infects multiple thymocyte subsets bearing the CD4 receptor (CD3$^+$ CD4$^+$ CD8$^-$, CD3$^{+/-}$ CD4$^+$ CD8$^+$. and CD3$^-$ CD4$^+$ CD8$^-$ cells) (23, 42). In these animals, X4 or R5/X4 HIV-1 strains replicated to higher levels and caused significantly more thymocyte depletion than non-syncytium-inducing R5 virus isolates (7, 8, 24).

In contrast to these animal experiments, several reports have indicated that in vitro, all cultured human CD4$^+$ thymocyte subsets are infectible by HIV-1 (17, 44, 45). However, a recent report, employing a coculture system consisting of thymic epithelial cells plus autologous thymocytes, clearly indicated that mature, single positive CD4 cells were the only CD4$^+$ thymocyte subpopulation able to sustain high levels of virus production (9). No HIV-1 replication was demonstrable in immature CD4$^+$ thymocyte lineages, including CD3$^{+/-}$ CD4$^+$ CD8$^+$ and CD3$^-$ CD4$^+$ CD8$^-$ cells. These latter findings are consistent with the results obtained in SHIV$_{DH12R}$-infected rhesus monkeys, where virtually all of the virus-producing cells were found in the thymic medulla, a region known to be enriched for mature thymocytes.

One of the more important issues that we wished to address was to identify the mechanism underlying the extraordinarily rapid and irreversible loss of CD4$^+$ T lymphocytes induced by highly pathogenic SHIVs. Was virus-induced apoptosis or necrosis responsible for the CD4$^+$ T-cell depletion? Were uninfected "bystander" T cells eliminated in lymphoid tissues? Apoptotic cells have been difficult to demonstrate in vivo, even in tissues such as the thymus, in which large numbers of cells are continuously undergoing programmed cell death (37). Cells in the very early stages of dying by apoptosis may be recognized by macrophages at a stage when their plasma membranes appear to be structurally and functionally intact (38). Their engulfment by phagocytes well before the emergence of changes recognized by reagents used to detect apoptosis and the rapid degradation of cellular contents can greatly mask the full extent of cell loss, as revealed in the "snapshot" of stained histological specimens such as those shown in Fig. 5.

Nonetheless, the number of TUNEL-positive cells in the paracortical regions of lymph nodes rose substantially between days 3 and 10 postinfection, paralleling the increase in viral RNA-producing cells in the same lymph node compartment (compare the day 10 panels in Fig. 3 and 5). Although our experimental design did not permit us to conclude that the ISH-positive cells in lymphoid tissues were the only ones undergoing apoptosis, their morphology and location in the paracortex strongly suggested that a majority of the dying cells were very likely also virus positive. By day 14, when significant depletions of CD4$^+$ T cells had already occurred, fewer TUNEL-positive cells were seen, and several exhibited the size and morphological appearance of phagocytes. The presence of increased numbers of apoptotic cells in B-cell-rich germinal centers on day 10 might fulfill the definition of "bystander" effect, but some of these cells could be CD4$^+$ T lymphocytes (see the day 10 panel of Fig. 2) or are simply B cells dying as a consequence of antibody affinity maturation. Thus, while our results show an increase in the numbers of apoptotic cells in regions of lymph nodes in which robust virus replication occurs, we cannot exclude that other mechanisms of cell death which may contribute to the massive depletions of CD4$^+$ T lymphocytes were observed.

We previously reported that macrophages in lymphoid tissue, GI tract, liver, and kidney are able to sustain high levels of virus production following the resolution of the acute viral infection (19). The results of the present study provide little direct evidence that tissue macrophages become infected during the acute SHIV infection. Virus loads in the blood fall 100- to 1,000-fold from their peak on day 14, and the very few ISH-positive cells present in lymph nodes on day 21 had morphological characteristics typical of lymphocytes, not macrophages. Of note, however, was the massive increase in HAM56-positive macrophages in lymph node sections during this same period.

On day 7, a majority of these macrophages were present in germinal centers (Fig. 7), very likely phagocytosing maturing B cells or possibly presenting antigen. Over the next 2 weeks, this pattern changed markedly, with macrophages swarming throughout all lymph node compartments, including the paracortex. In ongoing experiments using confocal microscopy to monitor the cell types expressing viral RNA, we have identified infected macrophages in lymph node specimens by week 6 postinfection (T. Igarashi, unpublished data). Considering the enormous number of macrophages in T-cell areas of the lymph node on day 21 postinfection (Fig. 7), it is quite likely that they become infected during this very early period, perhaps as a consequence of removing dying T lymphocytes during the acute infection.

ACKNOWLEDGMENTS

Tatsuhiko Igarashi and Charles R. Brown contributed equally to this work.

We thank Elaine Jaffe and Michael Eckhaus for help in interpreting histopathological specimens, Randy Elkins for invaluable assistance in the animal experiments, and Boris Skopets and Marisa St. Claire for performing the perfusion and necropsy procedures.

REFERENCES

1. **Agus, D. B., C. D. Surh, and J. Sprent.** 1991. Reentry of T-cells to the adult thymus is restricted to activated T-cells. J. Exp. Med. **173:**1039–1046.
2. **Amadori, A., G. De Silvestro, R. Zamarchi, M. L. Veronese, M. R. Mazza, G. Schiavo, M. Panozzo, A. De Rossi, L. Ometto, J. Mous, et al.** 1992. CD4 epitope masking by gp120/anti-gp120 antibody complexes. A potential mechanism for CD4+ cell function down-regulation in AIDS patients. J. Immunol. **148:**2709–2716.
3. **Amara, R. R., F. Villinger, J. D. Altman, S. L. Lydy, S. P. O'Neil, S. I. Staprans, D. C. Montefiori, Y. Xu, J. G. Herndon, L. S. Wyatt, M. A. Candido, N. L. Kozyr, P. L. Earl, J. M. Smith, H. L. Ma, B. D. Grimm, M. L. Hulsey, J. Miller, H. M. McClure, J. M. McNicholl, B. Moss, and H. L. Robinson.** 2001. Control of a mucosal challenge and prevention of AIDS by a multiprotein DNA/MVA vaccine. Science **292:**69–74.
4. **Badley, A. D., J. A. McElhinny, P. J. Leibson, D. H. Lynch, M. R. Alderson, and C. V. Paya.** 1996. Upregulation of Fas ligand expression by human immunodeficiency virus in human macrophages mediates apoptosis of uninfected T lymphocytes. J. Virol. **70:**199–206.
5. **Barouch, D. H., S. Santra, J. E. Schmitz, M. J. Kuroda, T. M. Fu, W. Wagner, M. Bilska, A. Craiu, X. X. Zheng, G. R. Krivulka, K. Beaudry, M. A. Lifton, C. E. Nickerson, W. L. Trigona, K. Punt, D. C. Freed, L. Guan, S. Dubey, D. Casimiro, A. Simon, M. E. Davies, M. Chastain, T. B. Strom, R. S. Gelman, D. C. Montefiori, and M. G. Lewis.** 2000. Control of viremia and prevention of clinical AIDS in rhesus monkeys by cytokine-augmented DNA vaccination. Science **290:**486–492.
6. **Bergeron, L., and J. Sodroski.** 1992. Dissociation of unintegrated viral DNA accumulation from single-cell lysis induced by human immunodeficiency virus type 1. J. Virol. **66:**5777–5787.
7. **Berkowitz, R. D., K. P. Beckerman, T. J. Schall, and J. M. McCune.** 1998. CXCR4 and CCR5 expression delineates targets for HIV-1 disruption of T-cell differentiation. J. Immunol. **161:**3702–3710.
8. **Camerini, D., H. P. Su, G. Gamez-Torre, M. L. Johnson, J. A. Zack, and I. S. Chen.** 2000. Human immunodeficiency virus type 1 pathogenesis in SCID-hu mice correlates with syncytium-inducing phenotype and viral replication. J. Virol. **74:**3196–3204.
9. **Chene, L., M. T. Nugeyre, E. Guillemard, N. Moulian, F. Barre-Sinoussi, and N. Israel.** 1999. Thymocyte-thymic epithelial cell interaction leads to high-level replication of human immunodeficiency virus exclusively in mature $CD4^+$ $CD8^-$ $CD3^+$ thymocytes: a critical role for tumor necrosis factor and interleukin-7. J. Virol. **73:**7533–7542.
10. **Committee on Care and Use of Laboratory Animals.** 1985. Guide for the care and use of laboratory animals NIH 85-23. Department of Health and Human Services, Washington, D.C.
11. **Dewar, R. L., H. C. Highbarger, M. D. Sarmiento, J. A. Todd, M. B. Vasudevachari, R. T. Davey, Jr., J. A. Kovacs, N. P. Salzman, H. C. Lane, and M. S. Urdea.** 1994. Application of branched DNA signal amplification to monitor human immunodeficiency virus type 1 burden in human plasma. J. Infect. Dis. **170:**1172–1179.
12. **Endo, Y., T. Igarashi, Y. Nishimura, C. Buckler, A. Buckler-White, R. Plishka, D. S. Dimitrov, and M. A. Martin.** 2000. Short- and long-term clinical outcomes in rhesus monkeys inoculated with a highly pathogenic chimeric simian/human immunodeficiency virus. J. Virol. **74:**6935–6945.
13. **Finkel, T. H., G. Tudor-Williams, N. K. Banda, M. F. Cotton, T. Curiel, C. Monks, T. W. Baba, R. M. Ruprecht, and A. Kupfer.** 1995. Apoptosis occurs predominantly in bystander cells and not in productively infected cells of HIV- and SIV-infected lymph nodes. Nat. Med. **1:**129–134.
14. **Gandhi, R. T., B. K. Chen, S. E. Straus, J. K. Dale, M. J. Lenardo, and D. Baltimore.** 1998. HIV-1 directly kills CD4+ T-cells by a Fas-independent mechanism. J. Exp. Med. **187:**1113–1122.
15. **Gougeon, M. L., and L. Montagnier.** 1999. Programmed cell death as a mechanism of CD4 and CD8 T-cell deletion in AIDS. Molecular control and effect of highly active antiretroviral therapy. Ann. N. Y. Acad. Sci. **887:**199–212.
16. **Groux, H., G. Torpier, D. Monte, Y. Mouton, A. Capron, and J. C. Ameisen.** 1992. Activation-induced death by apoptosis in CD4+ T-cells from human immunodeficiency virus-infected asymptomatic individuals. J. Exp. Med. **175:**331–340.
17. **Hays, E. F., C. H. Uittenbogaart, J. C. Brewer, L. W. Vollger, and J. A. Zack.** 1992. In vitro studies of HIV-1 expression in thymocytes from infants and children. AIDS **6:**265–272.
18. **Hirsch, V. M., G. Dapolito, P. R. Johnson, W. R. Elkins, W. T. London, R. J. Montali, S. Goldstein, and C. Brown.** 1995. Induction of AIDS by simian immunodeficiency virus from an African green monkey: species-specific variation in pathogenicity correlates with the extent of in vivo replication. J. Virol. **69:**955–967.
19. **Igarashi, T., C. R. Brown, Y. Endo, A. Buckler-White, R. Plishka, N. Bischofberger, V. Hirsch, and M. A. Martin.** 2001. Macrophage are the principal reservoir and sustain high virus loads in rhesus macaques after the depletion of CD4+ T-cells by a highly pathogenic simian immunodeficiency virus/HIV type 1 chimera (SHIV): Implications for HIV-1 infections of humans. Proc. Natl. Acad. Sci. USA **98:**658–663.
20. **Igarashi, T., Y. Endo, G. Englund, R. Sadjadpour, T. Matano, C. Buckler, A. Buckler-White, R. Plishka, T. Theodore, R. Shibata, and M. Martin.** 1999. Emergence of a highly pathogenic simian/human immunodeficiency virus in a rhesus macaque treated with anti-CD8 mAb during a primary infection with a nonpathogenic virus. Proc. Natl. Acad. Sci. USA **96:**14049–14054.
21. **Joag, S. V., Z. Li, L. Foresman, E. B. Stephens, L. J. Zhao, I. Adany, D. M. Pinson, H. M. McClure, and O. Narayan.** 1996. Chimeric simian/human immunodeficiency virus that causes progressive loss of $CD4^+$ T-cells and AIDS in pig-tailed macaques. J. Virol. **70:**3189–3197.
22. **Kestler, H., T. Kodama, D. Ringler, M. Marthas, N. Pedersen, A. Lackner, D. Regier, P. Sehgal, M. Daniel, N. King, et al.** 1990. Induction of AIDS in rhesus monkeys by molecularly cloned simian immunodeficiency virus. Science **248:**1109–1112.
23. **Kitchen, S. G., C. H. Uittenbogaart, and J. A. Zack.** 1997. Mechanism of human immunodeficiency virus type 1 localization in CD4-negative thymocytes: differentiation from a CD4-positive precursor allows productive infection. J. Virol. **71:**5713–5722.
24. **Kitchen, S. G., and J. A. Zack.** 1997. CXCR4 expression during lymphopoiesis: implications for human immunodeficiency virus type 1 infection of the thymus. J. Virol. **71:**6928–6934.
25. **Kovalev, G., K. Duus, L. Wang, R. Lee, M. Bonyhadi, D. Ho, J. M. McCune, H. Kaneshima, and L. Su.** 1999. Induction of MHC class I expression on immature thymocytes in HIV-1-infected SCID-hu Thy/Liv mice: evidence of indirect mechanisms. J. Immunol. **162:**7555–7562.
26. **Lackner, A. A., P. Vogel, R. A. Ramos, J. D. Kluge, and M. Marthas.** 1994. Early events in tissues during infection with pathogenic (SIVmac239) and nonpathogenic (SIVmac1A11) molecular clones of simian immunodeficiency virus. Am. J. Pathol. **145:**428–439.
27. **Lifson, J. D., G. R. Reyes, M. S. McGrath, B. S. Stein, and E. G. Engleman.** 1986. AIDS retrovirus induced cytopathology: gianT-cell formation and involvement of CD4 antigen. Science **232:**1123–1127.
28. **Meyaard, L., S. A. Otto, R. R. Jonker, M. J. Mijnster, R. P. Keet, and F. Miedema.** 1992. Programmed death of T-cells in HIV-1 infection. Science **257:**217–219.
29. **Moss, A. R., and P. Bacchetti.** 1989. Natural history of HIV infection. AIDS **3:**55–61.
30. **Muro-Cacho, C. A., G. Pantaleo, and A. S. Fauci.** 1995. Analysis of apoptosis in lymph nodes of HIV-infected persons. Intensity of apoptosis correlates with the general state of activation of the lymphoid tissue and not with stage of disease or viral burden. J. Immunol. **154:**5555–5566.
31. **Nahmias, A. J., W. S. Clark, A. P. Kourtis, F. K. Lee, G. Cotsonis, C. Ibegbu, D. Thea, P. Palumbo, P. Vink, R. J. Simonds, and S. R. Nesheim.** 1998. Thymic dysfunction and time of infection predict mortality in human immunodeficiency virus-infected infants. CDC Perinatal AIDS Collaborative Transmission Study Group. J. Infect. Dis. **178:**680–685.
32. **Papiernik, M., Y. Brossard, N. Mulliez, J. Roume, C. Brechot, F. Barin, A. Goudeau, J. F. Bach, C. Griscelli, R. Henrion, et al.** 1992. Thymic abnormalities in fetuses aborted from human immunodeficiency virus type 1 seropositive women. Pediatrics **89:**297–301.
33. **Reimann, K. A., J. T. Li, R. Veazey, M. Halloran, I. W. Park, G. B. Karlsson, J. Sodroski, and N. L. Letvin.** 1996. A chimeric simian/human immunodeficiency virus expressing a primary patient human immunodeficiency virus type 1 isolate Env causes an AIDS-like disease after in vivo passage in rhesus monkeys. J. Virol. **70:**6922–6928.
34. **Rosenzweig, M., D. P. Clark, and G. N. Gaulton.** 1993. Selective thymocyte depletion in neonatal HIV-1 thymic infection. AIDS **7:**1601–1605.
35. **Rosenzweig, M., M. Connole, A. Forand-Barabasz, M. P. Tremblay, R. P. Johnson, and A. A. Lackner.** 2000. Mechanisms associated with thymocyte apoptosis induced by simian immunodeficiency virus. J. Immunol. **165:**3461–3468.
36. **Rutherford, G. W., A. R. Lifson, N. A. Hessol, W. W. Darrow, P. M. O'Malley, S. P. Buchbinder, J. L. Barnhart, T. W. Bodecker, L. Cannon, L. S. Doll, et al.** 1990. Course of HIV-I infection in a cohort of homosexual and bisexual men: an 11 year follow up study. Br. Med. J. **301:**1183–1188.
37. **Savill, J.** 1997. Recognition and phagocytosis of cells undergoing apoptosis. Br. Med. Bull. **53:**491–508.
38. **Savill, J. S., A. H. Wyllie, J. E. Henson, M. J. Walport, P. M. Henson, and C. Haslett.** 1989. Macrophage phagocytosis of aging neutrophils in inflammation. Programmed cell death in the neutrophil leads to its recognition by macrophages. J. Clin. Investig. **83:**865–875.
39. **Schuurman, H. J., W. J. Krone, R. Broekhuizen, J. van Baarlen, P. van Veen, A. L. Golstein, J. Huber, and J. Goudsmit.** 1989. The thymus in acquired immune deficiency syndrome. Comparison with other types of immunodeficiency diseases, and presence of components of human immunodeficiency virus type 1. Am. J. Pathol. **134:**1329–1338.

40. **Shibata, R., F. Maldarelli, C. Siemon, T. Matano, M. Parta, G. Miller, T. Fredrickson, and M. A. Martin.** 1997. Infection and pathogenicity of chimeric simian-human immunodeficiency viruses in macaques: determinants of high virus loads and CD4 cell killing. J. Infect. Dis. **176:**362–373.
41. **Stanley, S. K., J. M. McCune, H. Kaneshima, J. S. Justement, M. Sullivan, E. Boone, M. Baseler, J. Adelsberger, M. Bonyhadi, J. Orenstein, et al.** 1993. Human immunodeficiency virus infection of the human thymus and disruption of the thymic microenvironment in the SCID-hu mouse. J. Exp. Med. **178:**1151–1163.
42. **Su, L., H. Kaneshima, M. Bonyhadi, S. Salimi, D. Kraft, L. Rabin, and J. M. McCune.** 1995. HIV-1-induced thymocyte depletion is associated with indirect cytopathogenicity and infection of progenitor cells in vivo. Immunity **2:**25–36.
43. **Surh, C. D., J. Sprent, and S. R. Webb.** 1993. Exclusion of circulating T-cells from the thymus does not apply in the neonatal period. J. Exp. Med. **177:** 379–385.
44. **Tanaka, K. E., W. C. Hatch, Y. Kress, R. Soeiro, T. Calvelli, W. K. Rashbaum, A. Rubinstein, and W. D. Lyman.** 1992. HIV-1 infection of human fetal thymocytes. J. Acquir. Immune Defic. Syndr. **5:**94–101.
45. **Uittenbogaart, C. H., D. J. Anisman, B. D. Jamieson, S. Kitchen, I. Schmid, J. A. Zack, and E. F. Hays.** 1996. Differential tropism of HIV-1 isolates for distinct thymocyte subsets in vitro. AIDS **10:**F9–16.
46. **Wang, L., G. R. Klimpel, J. M. Planas, H. Li, and M. W. Cloyd.** 1998. Apoptotic killing of CD4+ T lymphocytes in HIV-1-infected PHA-stimulated PBL cultures is mediated by CD8+ LAK cells. Virology **241:**169–180.
47. **Wykrzykowska, J. J., M. Rosenzweig, R. S. Veazey, M. A. Simon, K. Halvorsen, R. C. Desrosiers, R. P. Johnson, and A. A. Lackner.** 1998. Early regeneration of thymic progenitors in rhesus macaques infected with simian immunodeficiency virus. J. Exp. Med. **187:**1767–1778.
48. **Yoffe, B., D. E. Lewis, B. L. Petrie, C. A. Noonan, J. L. Melnick, and F. B. Hollinger.** 1987. Fusion as a mediator of cytolysis in mixtures of uninfected CD4+ lymphocytes and cells infected by human immunodeficiency virus. Proc. Natl. Acad. Sci. USA **84:**1429–1433.